# Fast and pure phase-shifting off-axis holographic microscopy with a digital micromirror device

Alexey Brodoline, Daniel Alexandre, Michel Gross

# Fast and pure phase-shifting off-axis holographic microscopy with a digital micromirror device

Alexey Brodoline[1,*], Daniel Alexandre[1], and Michel Gross[1]

[1]Laboratoire Charles Coulomb (L2C), Université Montpellier, CNRS, Montpellier, France

[*]Corresponding author: alexey.brodoline@gmail.com

**Abstract**

We present a phase-shifting digital holographic microscopy technique, where a digital micromirror device enables to perform a precise phase-only shift of the reference wave. By coupling the beam into a monomode fiber, we obtain a laser mode with a constant phase shift, equally acting on all pixels of the hologram. This method has the advantage of being relatively simple and compatible with high frame rate cameras, which makes it of great interest for the observation of fast phenomena. We demonstrate the validity of the technique in an off-axis configuration by imaging living *paramecia caudata*.

This is an author version of the manuscript. To access the Visualizations files please consult the original version published in Applied Optics (May 2022). https://doi.org/10.1364/AO.452382

**Citation:** A. Brodoline, D. Alexandre, and M. Gross, "Fast and pure phase-shifting off-axis holographic microscopy with a digital micromirror device", Appl. Opt. 61, 4296-4302 (2022).

# 1 Introduction

Since its invention by Dennis Gabor [1], and the emergence of digital recording and processing tools [2, 3], holography has become a widely used technique for absorption and phase imaging [4, 5, 6, 7]. The hologram is the result of interference between the optical wavefront scattered by the imaged object and a known reference wave. The complex spatial information about the optical field is encoded in the hologram and can be decomposed in three diffraction terms: the intensity zero order, the interference +1 order, proportional to the object field, and its complex conjugate -1 order.

In the Gabor inline configuration, the three orders overlap in frequency space, and the so-called twin image appears at reconstruction. This additional defocused image of the object can be an issue in some applications [8, 9, 10]. Computational solutions were developed for twin image suppression as iterative phase retrieval algorithms [11] or inverse problem approaches [12].

Prior to these numerical solutions, Leith and Upatnieks proposed the off-axis holography configuration [13], where an angle is introduced between the object and the reference beams. In this way, the three orders are spatially separated in Fourier space, and the +1 term can be isolated and numerically reconstructed [14], giving direct access to the complex optical field. The drawback is that a large part of the spatial frequency bandwidth is occupied by the zero order, whose etendue is the double of the etendue of the other orders. Some resolution or field of view has to be sacrificed to prevent the orders from overlapping. Several experimental [15, 16] and iterative numerical [17, 18, 19, 20] methods were proposed to attenuate the zero order and free more bandwidth for the interference terms. In [21], both zero and -1 orders are eliminated by a Fresnelet transform based algorithm.

Another solution for a reconstruction without twin image artifacts is the phase-shifting holography first introduced by Yamaguchi and Zhang [22, 23]. The illumination and reference beams follow separate paths and a controlled phase shift is applied to the reference wave. A series of holograms with specific phase shifts is acquired, and a linear combination of those enables to eliminate the zero and the -1 orders.

In the first demonstration of phase-shifting holography, a piezoelectric transducer (PZT) was used to translate a mirror and vary the optical path of the reference beam. For four positions of the mirror, four holograms with a $\pi/2$ phase shift between each were recorded. The PZT needs, however, to be calibrated to realize a precise phase shift. Some techniques using wave plates as phase retarders demonstrated reconstructions of static objects from only two holograms [24, 25]. A spatial light modulator (SLM) is another relevant tool for phase-shifting techniques since it can directly control the phase of the wavefront with a liquid crystal matrix [26, 27]. For example, an SLM was used to achieve phase-shifting holography at multiple wavelengths [28]. These devices are nonetheless expensive and relatively slow. Acousto-optic modulators (AOMs) were also proposed to perform phase-shifting holography [29, 30]. An AOM acts as a moving phase grating that imposes to the light passing trough a wave vector $d\boldsymbol{k}$ and a temporal frequency $d\omega$ shift at the acoustic

scale. This technique allows a precise and much faster phase control than previous ones, making it compatible with high acquisition frame rates (>100 Hz). Since the observation of fast phenomena with digital holography is a relevant issue, fast phase-shifting methods are of great interest. The method is, however, relatively hardware heavy and expensive, since it necessitates to use two AOMs with two RF power amplifiers and two signal generators synchronized with the camera.

We show that a digital micromirror device (DMD) can be used to perform phase-shifting holography at a high frame rate. The micromirror matrix of this electronic device enables to display binary patterns by individually switching the mirrors between two "on" and "off" tilted positions. Thus, the DMD can control the phase of the reflected beam by amplitude modulation. The advantages of such a device are its mechanical stability, low cost and most of all its high commutation speed which can reach several tens of kHz, orders of magnitude faster than regular SLMs [31]. For example, a DMD was used in optical tomography to obtain precise and stable control of the illumination beam angle by changing the orientation of the displayed grating [32, 33]. Closer to our configuration, a DMD was employed in an inline lensless setup in order to project phase-shifting fringes directly onto the imaged object [34]. The phase-shifting capability of the DMD through the Lee hologram method [35] was exploited in other configurations to determine the transmission matrix of a turbid medium [36] or to phase-encode the illumination for single pixel holography [37].

In this paper, we focus on the fast imaging capability and show that a DMD can perform phase-shifting holography in the case of mobile objects by homogeneously changing the phase of the reference beam. We demonstrate it in an off-axis microscope configuration by imaging living *paramecia caudata*. This method is, however, valid for any phase-shifting holographic setup (lensless, on-axis). We adopted the off-axis configuration because it better illustrates the suppression of the zero and -1 orders and is advantageous for imaging of moving objects. Also, this configuration allows a sensitivity at shot-noise level [38].

## 2 Phase-shifting principle

Let us first recall the theory of phase-shifting holography. During hologram acquisition, the camera records the interference pattern between the signal wave scattered by the object $E_S$ and a reference wave $E_R$. These two waves are complex fields with an amplitude and a phase: $E_S = a_S e^{i\varphi_S}$ and $E_R = a_R e^{i\varphi_R}$. For writing simplicity, the dependencies of the quantities on the position $(x, y)$ on the camera sensor are omitted. The intensity in the sensor plane corresponds to

$$\begin{aligned} I &= |E_S + E_R|^2 \\ &= a_S^2 + a_R^2 + a_S a_R e^{i(\varphi_S - \varphi_R)} + a_S a_R e^{-i(\varphi_S - \varphi_R)} \\ &= a_S^2 + a_R^2 + 2 a_S a_R \cos(\varphi_S - \varphi_R). \end{aligned} \tag{1}$$

In its fully developed form, the hologram appears as a sum of three terms, corresponding to the three orders: the intensity zero order $a_S^2 + a_R^2$, the +1 order $a_S a_R e^{i(\varphi_S - \varphi_R)}$ proportional to the field scattered by the object, and the twin complex conjugate -1 order $a_S a_R e^{-i(\varphi_S - \varphi_R)}$.

In phase-shifting holography, an additional controlled phase shift $\varphi_m$ has to be applied to the reference or the signal path to cancel the zero and -1 orders. Usually, four holograms are recorded [22], with a phase shift of $\pi/2$ between each other. In our setup the phase shift is applied to the reference beam. In this case the hologram becomes

$$I_m = a_S^2 + a_R^2 + 2a_S a_R \cos(\varphi_S - \varphi_m - \varphi_R), \tag{2}$$

where $\varphi_m = m\pi/2$ with $m = 0, 1, 2$ or 3. The four holograms are then sequentially recorded by the camera and linearly combined to eliminate the zero and the twin terms:

$$I_{4\varphi} = (I_0 - I_2) + i(I_1 - I_3) = 4a_S a_R e^{i(\varphi_S - \varphi_R)}. \tag{3}$$

The object amplitude and phase can be finally retrieved from the off-axis compensated field by the following formulas

$$a_S = \frac{1}{4a_R}\sqrt{\mathrm{Re}(I_{4\varphi})^2 + \mathrm{Im}(I_{4\varphi})^2}, \tag{4}$$

$$\varphi_S = \varphi_R + \mathrm{atan2}(\mathrm{Im}(I_{4\varphi}), \mathrm{Re}(I_{4\varphi})), \tag{5}$$

where Re() and Im() stand for real and imaginary parts, respectively, and atan2 is the four-quadrant inverse tangent.

To retrieve the signal field $a_S e^{i\varphi_S}$, the reference field amplitude $a_R$ and phase $\varphi_R$, which are slowly varying, have to be known. In practice, the amplitude is obtained by recording the intensity $a_R^2$ of the reference beam alone while the illumination is occluded. For the phase, the reconstruction is done with $\varphi_S - \varphi_R$, which means that the reference phase is mixed with the object field. As we will see, the effect of $\varphi_R$ can be numerically compensated for during the reconstruction procedure [39].

Figure 1 describes the principle of phase-shifting holography with a DMD. The device can display only binary intensity images, and the phase shift is achieved via amplitude modulation. A grating is formed by the micromirror array and transforms the incident laser beam into a reflected diffraction pattern. Since the mirrors are tilted in two "on" and "off" positions, the DMD produces two diffraction patterns in two directions. We work only with one of these patterns and select within it the +1 order diffracted beam. As illustrated, the DMD displays a one-dimensional grating with a periodicity of four pixels. The grating is translated by one pixel at every camera frame to produce an exact $\pi/2$ phase shift without calibration. The patterns are 11 00 11 00..., 01 10 01 10..., 00 11 00 11... and 10 01 10 01... The +1 diffraction order of the beam that undergoes a phase shift $\varphi_m$ is used as reference. In this case, the phase, but not the amplitude, of the entire laser

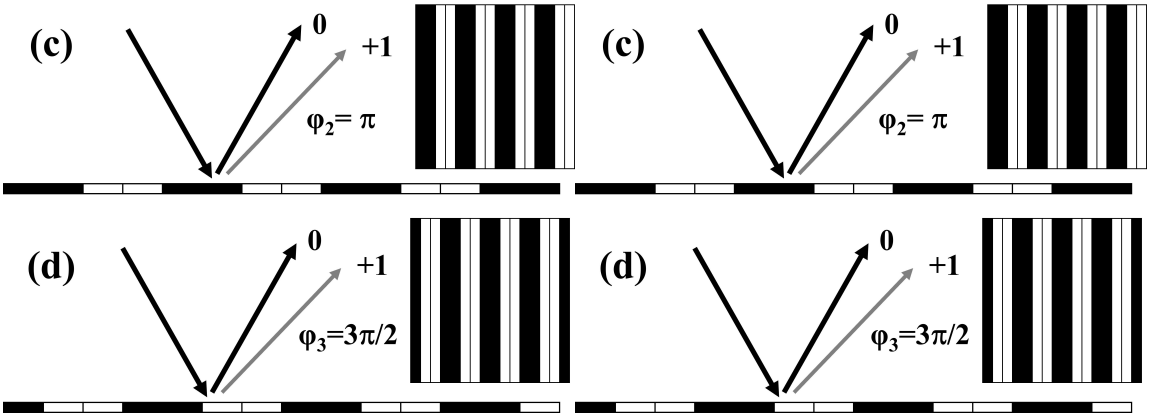


Figure 1: Four patterns displayed on the DMD to achieve phase-shifting holography. The +1 diffraction order undergoes a phase shift $\varphi_m$ whose value is modified by the translation of the binary grating. The patterns correspond to (a) $m = 0$, (b) $m = 1$, (c) $m = 2$ and (d) $m = 3$.

mode of the reference beam is shifted. On the contrary, in the configuration presented by *Zhou et al.* [34], the zero order diffracted beam was used, and the phase shift came from the spatial shift of the structured illumination pattern projected on the object by the DMD. The phase-shift can therefore be pixel dependent. Moreover, because of the one-path configuration, the relative phase shift was not controlled.

## 3 Experimental implementation

The experimental setup is depicted in Fig. 2. It is based on an upright optical microscope that has been adapted for digital holography. The light emitted by a laser diode L (HL6545MG: 120 mW, 660 nm) is separated in two by a beamsplitter BS. One part is directed toward the micromirror matrix of the DMD (DLP3000, DLP LightCrafter EVM). The device displays successively four horizontal binary gratings with a period of four pixels. The gratings are vertically shifted by one pixel to perform a $\pi/2$ shift. The DMD matrix produces several diffraction orders, where the zero, +1 and -1 are the brightest ones. A set of apertures and mirrors can be used to select the +1 phase-shifted order. It contains around 4% of the light incident on the DMD. The beam is then injected into a monomode optical fiber that acts as a spatial filter and generates a spherical reference wave $E_R$. The DMD phase shift affects the entire laser mode and, thus, is constant for all camera pixels.

The second part of the laser beam is injected into the illumination path of the microscope with a set of mirrors M. The object is illuminated by a plane wave and produces the scattered signal field $E_S$. A negative 1951 USAF resolution test chart plays the role

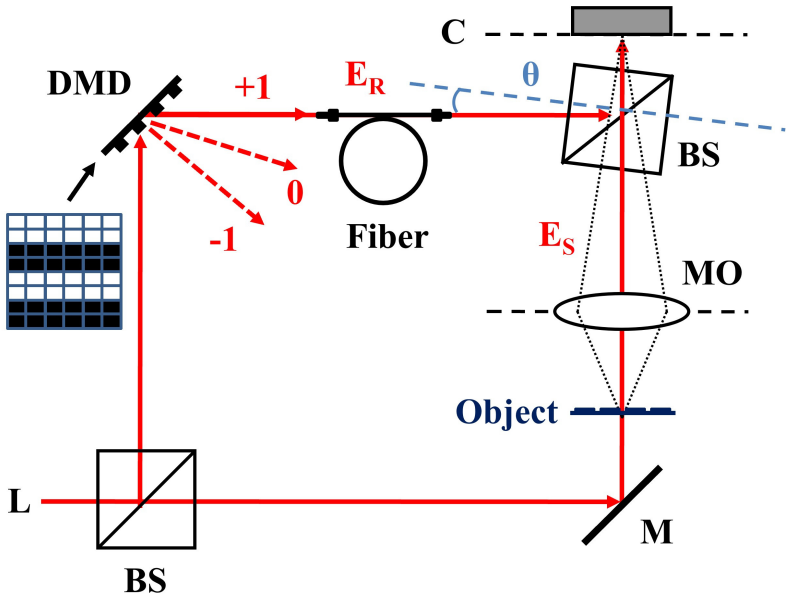


Figure 2: Outline of the off-axis DMD phase-shifting digital holographic microscopy setup. L: laser diode, BS: beam splitter, DMD: digital micromirror device, $E_R$: reference wave, M: mirror, MO: microscope objective, $E_S$: scattered wave, $\theta$: off-axis angle, C: camera.

of a test object. A microscope objective MO (Nikon 4x/NA=0.1, air) is used to image the object on the camera plane C. The effective magnification of the system of 11.6x is directly measured with the resolution test chart.

A second BS, tilted with an angle $\theta$ in order to achieve off-axis holography, combines the reference and signal beams. The camera is a Mikrotron EoSens CL ($1280 \times 1024$ pixels, 14 µm) acquiring at 200 Hz for a 10-bit dynamic range and with a 20 ms exposure time. While the DMD can reach 4 kHz, the output frame rate is limited by the camera characteristics and is reduced to 50 Hz due to the four-phases combination. The method is nonetheless compatible with higher frame rate cameras. The camera generates a digital output signal that is used as an input trigger by the DMD to synchronize the camera acquisition with the pattern display. Figure 2 does not depict neutral density filters and polarizers used to adjust the intensities on both arms in order to not saturate the image sensor. The optical power of the illumination and reference beams is of several tens of microwatts.

Since the reference $E_R$ is a spherical wave, its wavefront curvature has to be compensated for. This is done by adjusting the position of the optical fiber end to make the $E_R$ wave curvature to be roughly cancelled by the effect of propagation of the signal wave $E_S$ from the MO rear pupil to the camera. The hologram can then be multiplied by a quadratic phase mask for finer correction [39]. Figure 3(a) shows the Fourier transform

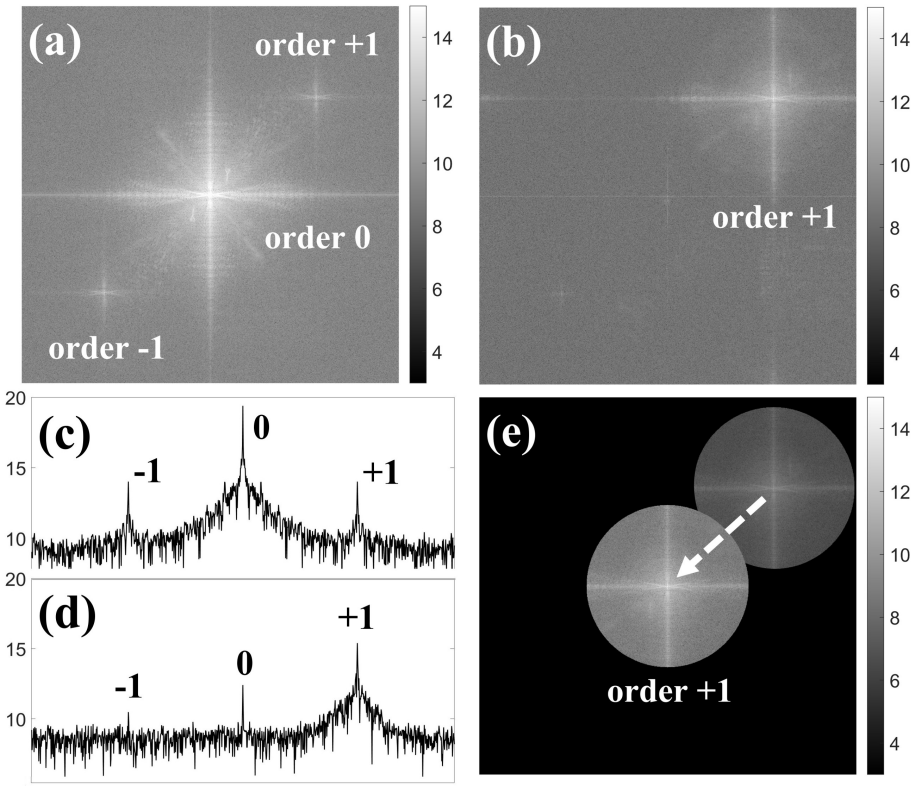


Figure 3: (a) Fourier transform of a hologram of a negative 1951 USAF resolution test chart. (b) Fourier transform after combination of four phase-shifted holograms. Only the +1 order remains. (c) Spectrum profile of a single hologram. (d) Spectrum profile in the case of phase-shifting. (e) Illustration of the filtering of the +1 order with a circular mask and compensation of the off-axis angle. Logarithm of the modulus is represented.

of a hologram of the 1951 USAF resolution test chart. The logarithm of the modulus is represented for clarity. Due to the off-axis configuration, the three hologram components are distinctly visible, with the zero order being dominant in terms of occupied bandwidth and energy. The more the wavefront curvature compensation is accurate, the more the diffraction orders appear sharp. The profile giving the spectrum value at every pixel along a diagonal line passing by the centers of the three orders is depicted in Fig. 3(c).

After reference calibration, a series of holograms phase-shifted by the DMD is recorded. The combination of each group of four consecutive holograms according to (3) allows to cancel the zero and -1 orders. This can be clearly seen with the Fourier transform of $I_{4\varphi}$ in Fig. 3 (b). The corresponding spectrum profile is given in Fig. 3 (d). Most of the energy is now contained in the +1 order, and its peak value is increased by a factor of 20. The

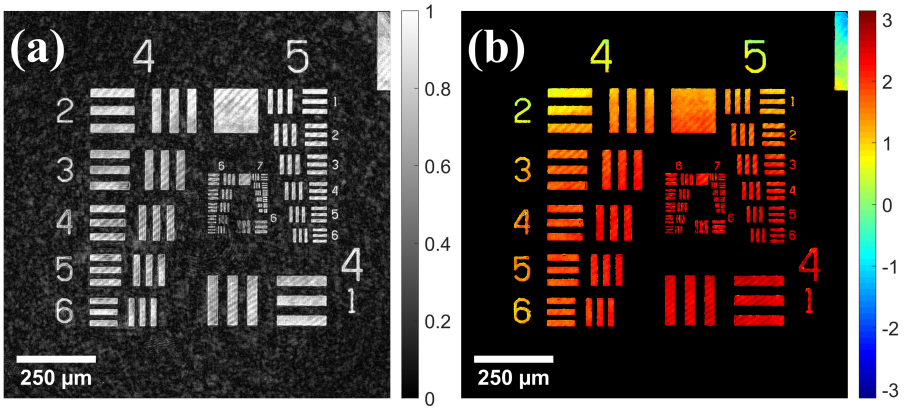


Figure 4: Images of a negative 1951 USAF resolution test chart reconstructed from four holograms phase-shifted by the DMD. (a) Amplitude and (b) phase. For clarity, a mask was applied to the opaque region on the phase map. Scale bar is 250 µm.

phase-shift of $\pi/2$ of the reference beam is thus successfully achieved with the DMD. The remaining zero order peak is due to low frequency noise specific to our camera sensor and is also present in the absence of any illumination.

The +1 order is then cropped with a circular mask and copied in the center of the reconstruction grid according to the classic procedure [14], compensating for the off-axis angle, as schematized in Fig. 3 (e). The radius of the filter corresponds to an angular spatial frequency of 1.12 rad.µm$^{-1}$ and allows to capture the high frequencies of the signal.

After an inverse Fourier transform, the hologram can be reconstructed according to equations (4) and (5). Figures 4 (a) and (b) give, respectively, the reconstructed amplitude $a_S$ and phase difference $\varphi_S - \varphi_R$ of the USAF target in the camera conjugate plane. Even if the reference phase $\varphi_R$ is not exactly known, the reconstructed phase is supposed to be as flat as possible after curvature and off-axis compensation. A slow phase variation is nonetheless noticeable on Fig. 4 (b). Since the resolution test chart is negative, the region outside the patterns is completely opaque. The phase is not defined in this area and is reconstructed as random. For the clarity of the figure, a mask was applied to this region. The fringes visible in the reconstructions are due to unwanted interferences in the glass plate recovering the camera sensor.

To highlight the advantage of the combination of off-axis with phase-shifting holography, we show in Fig. 5 the amplitude reconstructed from the same hologram but by simple filtering of the +1 order term [Fig. 3 (a)], without the phase-shifting procedure. Figure 5 (a) shows the amplitude reconstructed with the same filtering radius of 1.12 rad.µm$^{-1}$ as previously. In this case, some high frequencies of the zero order end up in the cropped region. Thus, the reconstruction presents several artifacts, mainly coming from parasitic reflections of the reference beam (which is therefore not a perfect plane wave). In addition,

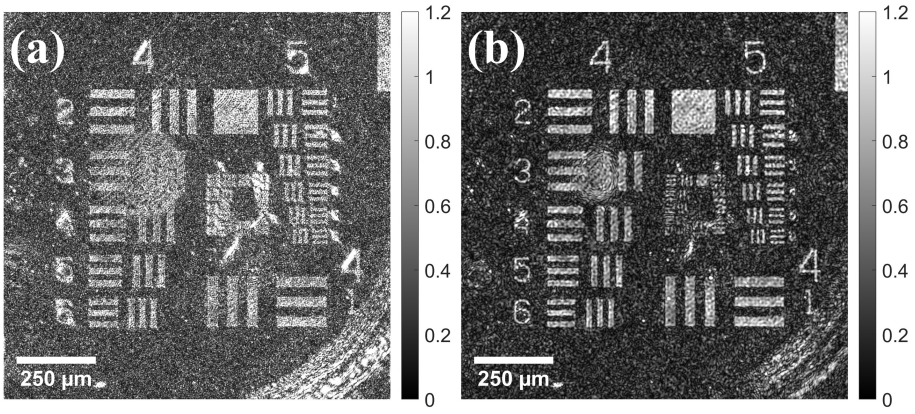


Figure 5: Negative 1951 USAF resolution test chart amplitude reconstructed by classical off-axis holography without phase-shifting method. Filter frequency radius of (a) 1.12 rad.µm$^{-1}$ and (b) 0.61 rad.µm$^{-1}$. Scale bar is 250 µm.

the smallest elements of the resolution test chart are indiscernible. The zeroth order noise can be reduced by decreasing the Fourier cutoff frequency, as it is shown in Fig. 5 (b) obtained with a filter radius of 0.61 rad.µm$^{-1}$. However, a trade-off between the total artifact removal and the loss of the highest frequencies of the relevant signal needs to be made, as can be observed on the corners of the chart elements.

To validate the ability of the DMD phase-shifting method to remove the zero and -1 orders, we reduced the off-axis angle $\theta$ to zero and performed an on-axis phase-shifting experiment. We should remark what the illumination conditions (intensity, wave curvature) were not exactly the same as in the previous configuration. The Fourier transform of an on-axis hologram of the resolution test chart is shown in Fig. 6 (a): the three diffraction orders overlap at the zero frequency. After combination of four phase-shifted holograms, only the +1 order remains, as can be seen in Fig. 6 (b). The reconstructed amplitude in Fig. 6 (c) shows a clear image of the resolution test chart without strong artifacts, meaning that the zero and -1 orders were successfully cleaned. This result can be compared to a reconstruction obtained in the same illumination conditions, but in a phase-shifting off-axis configuration, presented in Fig. 6 (d). As can be seen, there is no major difference in resolution between the two images. The on-axis reconstruction has, however, a higher definition. Indeed, since the +1 order is located in the center of the reconstruction grid, the cropped area was expanded to a cutoff frequency of 2.53 rad.µm$^{-1}$, increasing the number of pixels, while its is still of 1.12 rad.µm$^{-1}$ in the off-axis case. It would be also possible to optimize the bandwidth by bringing the camera closer to the MO and make the +1 order occupy all the Fourier space. However, in our setup, it would reduce the magnification and make the on/off-axis comparison less direct.

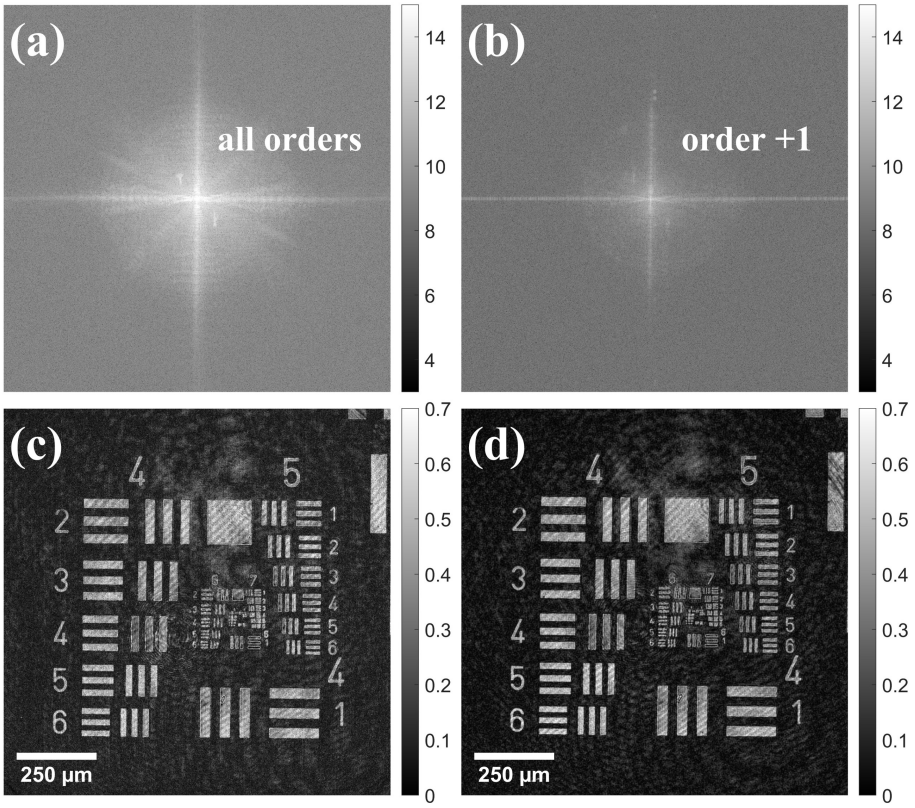


Figure 6: (a) Fourier transform of an on-axis hologram of the resolution test chart. (b) Fourier transform after phase-shifting. Only the +1 order remains. (c) Reconstructed amplitude in the on-axis phase-shifting configuration. Filtering at 2.53 rad.µm$^{-1}$. (d) Reconstructed amplitude in the off-axis phase-shifting configuration. Filtering at 1.12 rad.µm$^{-1}$. Scale bar is 250 µm.

The temporal stability of the method was tested by imaging a blank microscope slide. While the DMD was carrying out the phase-shift, every frame was reconstructed by simple off-axis holography. We calculated the mean phase value $\overline{\varphi}$ on a flat phase area of 500x500 pixels:

$$\overline{\varphi}(t_n) = \frac{1}{N^2} \sum_{x,y=1}^{N} \text{atan2}(\text{Im}(I(x,y,t_n)), \text{Re}(I(x,y,t_n))), \tag{6}$$

where $I$ is the filtered and off-axis compensated hologram, $x, y$ are the pixel indexes, $t_n$ is the camera frame count and $N$=500. Then we calculated the mean phase difference between adjacent camera frames:

$$\Delta\overline{\varphi}(t_n) = \overline{\varphi}(t_n + 1) - \overline{\varphi}(t_n). \tag{7}$$

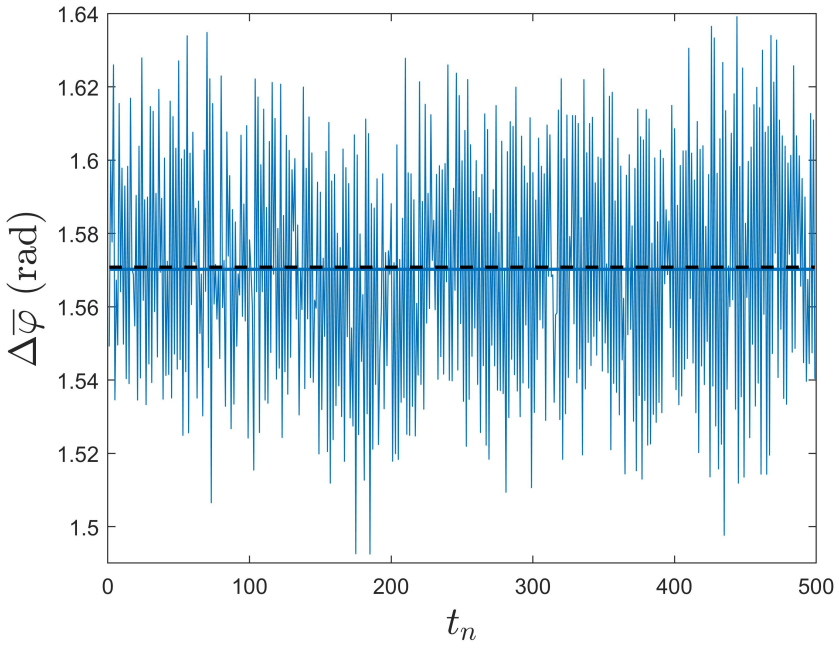


Figure 7: Mean phase difference between consecutive, DMD phase-shifted holograms of a blank microscope slide, calculated on a 500x500 pixels region, as a function of the frame number. The mean value over 500 frames (blue straight line) is 1.5702 rad and the standard deviation is 0.0341 rad. The black dashed line represents $\pi/2 \simeq 1.5708$ rad.

Figure 7 shows that the phase difference remains close to the expected $\pi/2 \simeq 1.5708$ rad shift. The experimental value measured over 500 frames is $1.5702 \pm 0.0341$ rad. The temporal phase variations ($\sim 2\%$) are of the order of the noise of the experimental setup and can be due to air, laser or mechanical fluctuations.

## 4 Imaging of moving objects

The main advantage provided by the DMD is its capability to refresh diffraction patterns and to phase-shift the holograms at a fast rate. This is suitable for the reconstruction of the amplitude and the phase of moving objects. To illustrate this, we imaged *paramecia caudata*: about 200 µm in length unicellular organisms that use cilia for locomotion in water. *Paramecia* were cultivated during 10 days in aquarium water in order to obtain a dense population from an initial small group. A dry banana skin was used as the catalyst of bacteria growth, which served as nutrient for the *paramecia*. Afterwards, *paramecia* were prepared in water between a microscope slide and a coverslip. To diversify the imaged

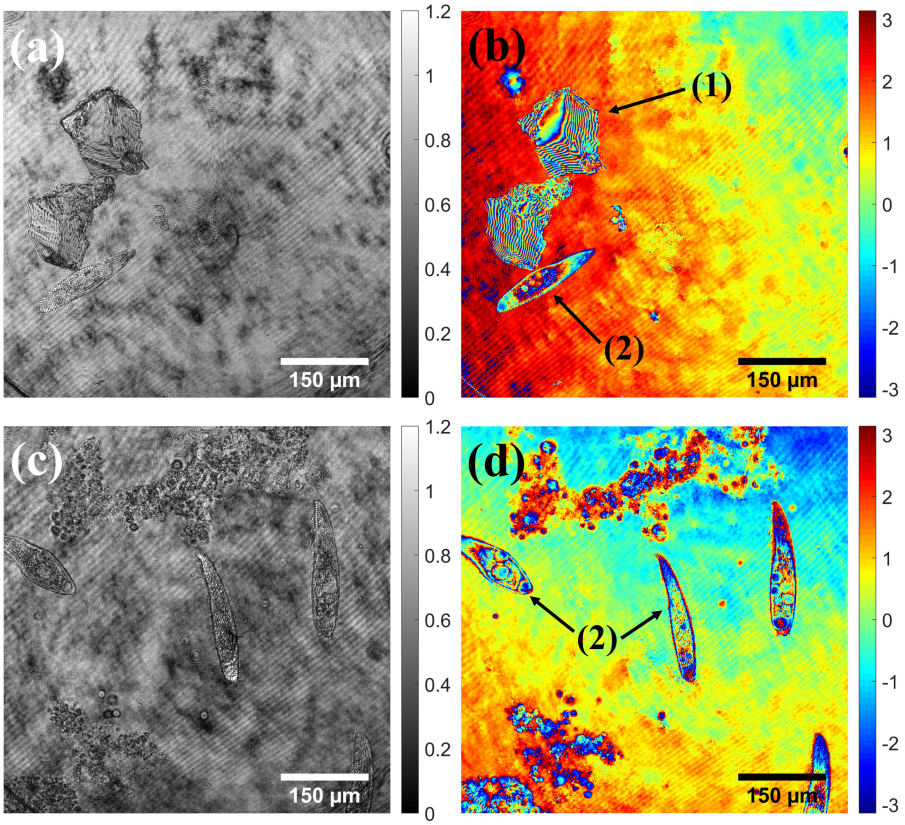


Figure 8: Images of microplastic (1) and *paramecium caudatum* (2) reconstructed from four DMD phase-shifted holograms. (a,c) Amplitude and (b,d) respective phase. Scale bar is 150 µm.

objects, we also added microparticles (¡200 µm) of polybutylene succinate adipate (PBSA). They were prepared by cryogenic grinding from 130 µm thickness polymer films.

Two reconstructed holograms are represented in Fig. 8, with the corresponding amplitude (a,c) and wrapped phase (b,d). The microscope setup is identical, but we reach an effective magnification of 21.7x with an Olympus (10x/NA=0.3, air) objective. Figures 8 (a,b) show two particles of PBSA and a *paramecium caudatum*. Figures 8 (c,d) show a group of *paramecia* surrounded by some biological residues. The reconstructed amplitude is mostly transparent, while the phase images give information on the internal structure of the microorganisms. The locomotion of the *paramecia* in water using cilia is shown in Visualization 1 and Visualization 2. They were realized from a sequence of 508 phase-shifted holograms acquired at 200 Hz. For clarity, the video speed was reduced by two, reaching 25 Hz. The images from Figs. 8 (c,d) correspond to the 25th frame of the visualizations.

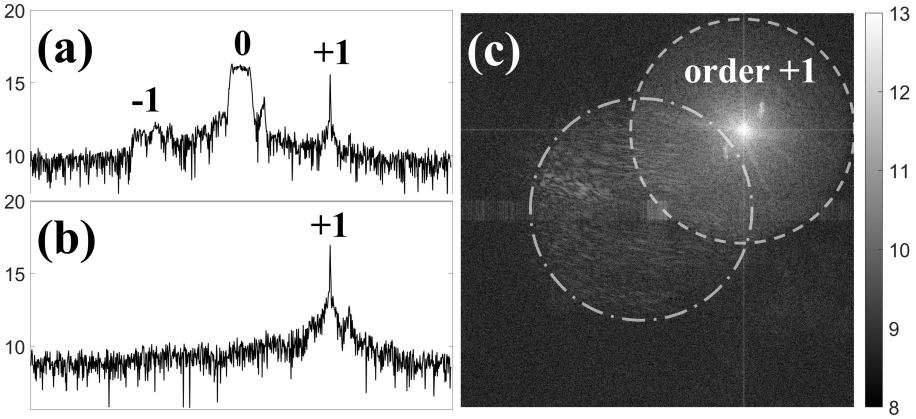


Figure 9: Spectrum profiles of *paramecia* holograms (a) without and (b) with phase-shifting holography. (c) Spectrum in the case of phase-shifting holography: +1 order (dashed circle) and zero order residue (dashed-dotted circle).

The Fourier transforms of the holograms of the *paramecia* are represented in Fig. 9. The spectrum profiles in the case of simple holography and in the case of the DMD phase-shifting holography are shown in Figs. 9 (a,b), respectively. The top hat aspect of the -1 and zero orders and the absence of the camera noise peak are due to the fact that we compensated for the reference field curvature for the +1 order with a spherical phase factor. By comparing the two profiles, we can tell that the cleaning of the zero and -1 terms is successful. Nonetheless, judging by Fig. 9 (c), it can be noticed that some residue surrounding the zeroth order region still remains. This residue is variable in time and is due to the movement of the *paramecia*. Indeed, our camera acquisition frame rate is too slow to keep the *paramecia* nearly immobile from one frame to another and realize a perfect cleaning of the terms $|E_S(t_n)|^2 - |E_S(t_n + 2)|^2$ according to (3). The remaining signal is weak, but still can be of the order of the highest frequencies of the +1 order. This does not affect notably our reconstructions (Fig. 8), but for the moving objects, their quality decreases if we increase the filtering radius of the +1 order. The off-axis configuration is therefore suitable in the case where the camera is not fast enough.

We illustrated this point by imaging fast and small (about 10 µm in diameter) ciliates. Their locomotion is more erratic than the one of the *paramecia caudata* and is accompanied by a spin movement. Figure 10 (a) shows the Fourier transform of a hologram of the ciliates after the phase-shifting procedure. The zero order exhibits a strong residue due to the movement of the microorganisms. The hologram acquisition was performed with two off-axis angles configurations. In the first one, the angle was large enough to avoid the superposition of the +1 order with the zero order residue, while in the second one, a part of the cropped +1 order mixed with the zero order. This last configuration corresponds to the Fig. 10 (a). The reconstructed amplitudes in the case of large and small off-axis

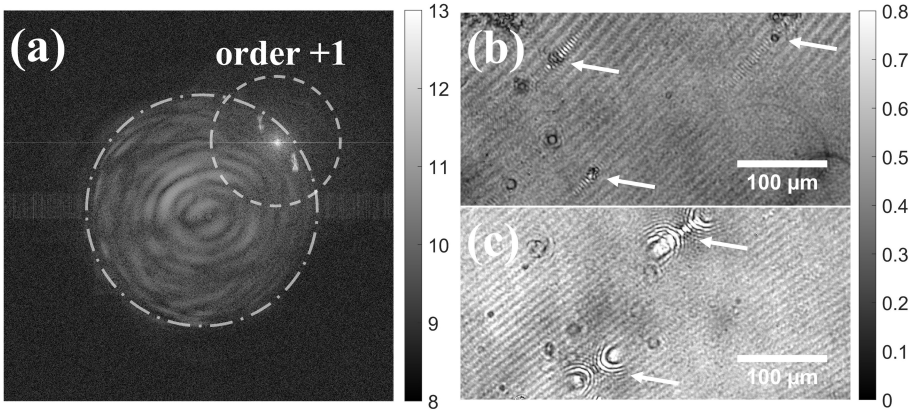


Figure 10: (a) Spectrum in the case of phase-shifting holography of small ciliates: +1 order (dashed circle) and zero order residue (dashed-dotted circle). (b) Amplitude reconstruction in the case of large off-axis angle. (c) Amplitude reconstruction in the case of small off-axis angle, corresponding to (a). The white arrows point to moving ciliates. Scale bar is 150 µm.

angles are shown in Figs. 10 (a) and (b), respectively. The image is zoomed in for better visibility. The white arrows point to several moving ciliates. The case where the zero and +1 orders overlap presents significant bow-tie shaped artifacts around the moving objects, which are strongly attenuated with the larger off-axis angle. We should remark that in this example the residue is strengthened by the fact what $E_R \simeq E_S$, while in Fig. 9 we have the $E_R \gg E_S$ condition. The artifacts can therefore be attenuated if the experiment allows it. The movement of the ciliates in the total field of view can be seen in Visualization 3 and Visualization 4, which give sequences of reconstructed amplitudes in both off-axis configurations. Figures 10 (b,c) correspond to frames 45 and 38, respectively. The video frame rate is 25 Hz.

## 5 Conclusion

In this paper, we demonstrated the capability of a digital micromirror device to perform fast phase-shifting holography and tested it in an off-axis configuration on a set of moving microscopic objects. A precise and pure phase shift of the reference beam is realized via amplitude modulation, by displaying on the DMD several translated binary gratings. The entire laser mode transmitted by the optical fiber undergoes the phase shift, which is thus constant for all pixels of the hologram. In our case, because of the camera characteristics, the output video frame rate is limited to 50 Hz, but with our model of DMD and a suitable camera, we could theoretically reach 1 kHz.

In our experiment, we focused on a combination of four patterns with a phase shift

of $\pi/2$. However, by changing the width in pixels of the displayed gratings, any desired phase shift can be obtained (*e.g.* $\pi/3$, $\pi/4$...). For example, the acquisition of $\pi/3$ phase-shifted holograms will reduce the amount of stored data necessary to reconstruct an image sequence.

In our configuration, the off-axis angle $\theta$ is large and the orders are well separated in frequency space. The summation of the +1 order filtering and the suppression of zero and -1 orders with phase-shifting holography allows to reach shot-noise sensitivity and avoid artifacts. Nonetheless, the method can as well be applied in the case where the orders overlap due to a smaller off-axis angle or a larger spectral etendue. The removing of the zero order with a linear combination of phase-shifted holograms will, however, be perfect, only if the observed object is motionless during the acquisition of these holograms. In this case, the zero order suppression algorithms could be complementary to the phase-shifting technique if the computing time is not an issue. They do not necessitate a sequence of holograms and are hence compatible with moving objects imaging.

The fast commutation speed of DMDs is therefore an advantage to image the amplitude and phase of moving objects. They are compatible with high frame rate cameras, which is not the case of piezoelectric transducers and spatial light modulators. The acousto-optic modulators that can be used with fast cameras require more hardware implementation and are more expensive. Hence, the DMD provides a way to realize a simple, fast, precise and cheap[1] phase-shifting setup. One drawback of the DMD is, nevertheless, its poor diffraction efficiency, which results in laser light power losses. However, this limitation is minimal since the total signal $E_S E_R^*$ depends on the power of the reference and the signal beams and in our experiment, both beams still need to be attenuated to not saturate the camera.

The phase-shifting technique with a DMD could also be extended to sideband holography [40]. It consists of adjusting the frequency of the reference wave to detect the holographic signal at a specific frequency, different from the illumination one. It can be done with a DMD by displaying a moving grating. It could be used to analyze vibrating objects and selectively detect the vibration sideband components.

**Funding** LabEx Numev (ANR-10-LABX-20: Micro Holo 4D); Centre National de la Recherche Scientifique (CNRS) "Défi: instrumentation aux limites 2018".

**Acknowledgements** The authors acknowledge Antigoni Theodoratou for the preparation of the PBSA microparticles.

**Disclosures** The authors declare no conflicts of interest.

**Data availability** Data underlying the results presented in this paper are not publicly available at this time but may be obtained from the authors upon reasonable request.

[1]The simplest DMD model DLP DLCR2000 EVM cost around 100$.

## References


[1] D. Gabor. A new microscopic principle. *Nature*, 161:777–778, 1948.

[2] J. W. Goodman and R. W. Lawrence. Digital image formation from electronically detected holograms. *Applied Physics Letters*, 11(3):77–79, 1967.

[3] U. Schnars and W. Jüptner. Direct recording of holograms by a ccd target and numerical reconstruction. *Applied optics*, 33(2):179–181, 1994.

[4] Arun Anand, Inkyu Moon, and Bahram Javidi. Automated disease identification with 3-d optical imaging: A medical diagnostic tool. *Proceedings of the IEEE*, 105(5):924–946, 2017.

[5] Yongkeun Park, Christian D. Depeursinge, and Gabriel Popescu. Quantitative phase imaging in biomedicine. *Nature Photonics*, 12:578–589, 2018.

[6] Yichen Wu, Yilin Luo, Gunvant R. Chaudhari, Yair Rivenson, Ayfer Calis, Kevin de Haan, and Aydogan Ozcan. Bright-field holography: cross-modality deep learning enables snapshot 3d imaging with bright-field contrast using a single hologram. *Light, Science & Applications*, 8, 2019.

[7] Daniele Pirone, Pasquale Memmolo, Francesco Merola, Lisa Miccio, Martina Mugnano, Amedeo Capozzoli, Claudio Curcio, Angelo Liseno, and Pietro Ferraro. Rolling angle recovery of flowing cells in holographic tomography exploiting the phase similarity. *Appl. Opt.*, 60(4):A277–A284, Feb 2021.

[8] Levent Onural and Peter D Scott. Digital decoding of in-line holograms. *Optical engineering*, 26(11):261124, 1987.

[9] KA Nugent. Twin-image elimination in gabor holography. *Optics communications*, 78(3-4):293–299, 1990.

[10] J. Garcia-Sucerquia, W. Xu, S.K. Jericho, P. Klages, M.H. Jericho, and H.J. Kreuzer. Digital in-line holographic microscopy. *Applied optics*, 45(5):836–850, 2006.

[11] J. R. Fienup. Phase retrieval algorithms: a comparison. *Appl. Opt.*, 21(15):2758–2769, Aug 1982.

[12] Fabien Momey, Loïc Denis, Thomas Olivier, and Corinne Fournier. From fienup's phase retrieval techniques to regularized inversion for in-line holography: tutorial. *J. Opt. Soc. Am. A*, 36(12):D62–D80, Dec 2019.

[13] E.N. Leith and J. Upatnieks. Reconstructed wavefronts and communication theory. *JOSA*, 52(10):1123–1130, 1962.

[14] E. Cuche, P. Marquet, and C. Depeursinge. Spatial filtering for zero-order and twin-image elimination in digital off-axis holography. *Applied optics*, 39(23):4070–4075, 2000.

[15] Yimo Zhang, Qieni Lü, and Baozhen Ge. Elimination of zero-order diffraction in digital off-axis holography. *Optics Communications*, 240(4):261–267, 2004.

[16] Jorge A. Herrera Ramírez and Jorge Garcia-Sucerquia. Digital off-axis holography without zero-order diffraction via phase manipulation. *Optics Communications*, 277(2):259–263, 2007.

[17] Gu-Liang Chen, Ching-Yang Lin, Ming-Kuei Kuo, and Chi-Ching Chang. Numerical suppression of zero-order image in digital holography. *Opt. Express*, 15(14):8851–8856, Jul 2007.

[18] Yanchao Dong and Jian Wu. Space-shifting digital holography with dc term removal. *Opt. Lett.*, 35(8):1287–1289, Apr 2010.

[19] Nicolas Pavillon, Cristian Arfire, Isabelle Bergoënd, and Christian Depeursinge. Iterative method for zero-order suppression in off-axis digital holography. *Opt. Express*, 18(15):15318–15331, Jul 2010.

[20] Zhonghong Ma, Lijun Deng, Yong Yang, Hongchen Zhai, and Qi Ge. Numerical iterative approach for zero-order term elimination in off-axis digital holography. *Opt. Express*, 21(23):28314–28324, Nov 2013.

[21] Michael Liebling, Thierry Blu, and Michael A. Unser. Nonlinear Fresnelet approximation for interference term suppression in digital holography. In Michael A. Unser, Akram Aldroubi, and Andrew F. Laine, editors, *Wavelets: Applications in Signal and Image Processing X*, volume 5207, pages 553 – 559. International Society for Optics and Photonics, SPIE, 2003.

[22] I. Yamaguchi and T. Zhang. Phase-shifting digital holography. *Optics letters*, 22(16):1268–1270, 1997.

[23] Ichirou Yamaguchi, Jun ichi Kato, Sohgo Ohta, and Jun Mizuno. Image formation in phase-shifting digital holography and applications to microscopy. *Appl. Opt.*, 40(34):6177–6186, Dec 2001.

[24] Pengyi Guo and Anthony J. Devaney. Digital microscopy using phase-shifting digital holography with two reference waves. *Opt. Lett.*, 29(8):857–859, Apr 2004.

[25] Natan T. Shaked, Yizheng Zhu, Matthew T. Rinehart, and Adam Wax. Two-step-only phase-shifting interferometry with optimized detector bandwidth for microscopy of live cells. *Opt. Express*, 17(18):15585–15591, Aug 2009.

[26] Yasuhiro Takaki, Hiroki Kawai, and Hitoshi Ohzu. Hybrid holographic microscopy free of conjugate and zero-order images. *Appl. Opt.*, 38(23):4990–4996, Aug 1999.

[27] Y. Awatsuji, A. Fujii, T. Kubota, and O. Matoba. Parallel three-step phase-shifting digital holography. *Applied Optics*, 45:2995–3002, 2006.

[28] Tatsuki Tahara and Yutaka Endo. Multiwavelength-selective phase-shifting digital holography without mechanical scanning. *Applied Optics*, 58(34):G218–G225, 2019.

[29] F. Le Clerc, L. Collot, and M. Gross. Numerical heterodyne holography with two-dimensional photodetector arrays. *Optics letters*, 25(10):716–718, 2000.

[30] M. Atlan, M. Gross, and E. Absil. Accurate phase-shifting digital interferometry. *Optics Letters*, 32:1456–1458, 2007.

[31] Sergey Turtaev, Ivo T. Leite, Kevin J. Mitchell, Miles J. Padgett, David B. Phillips, and Tomáš Čižmár. Comparison of nematic liquid-crystal and dmd based spatial light modulation in complex photonics. *Opt. Express*, 25(24):29874–29884, Nov 2017.

[32] S. Shin, K. Kim, J. Yoon, and YK. Park. Active illumination using a digital micromirror device for quantitative phase imaging. *Optics letters*, 40(22):5407–5410, 2015.

[33] KR. Lee, K. Kim, G. Kim, S. Shin, and YK. Park. Time-multiplexed structured illumination using a dmd for optical diffraction tomography. *Optics letters*, 42(5):999–1002, 2017.

[34] Wenjing Zhou, Qiangsheng Xu, Yingjie Yu, and Anand Asundi. Phase-shifting in-line digital holography on a digital micro-mirror device. *Optics and lasers in engineering*, 47(9):896–901, 2009.

[35] Wai-Hon Lee. Binary synthetic holograms. *Appl. Opt.*, 13(7):1677–1682, Jul 1974.

[36] Donald B. Conkey, Antonio M. Caravaca-Aguirre, and Rafael Piestun. High-speed scattering medium characterization with application to focusing light through turbid media. *Opt. Express*, 20(2):1733–1740, Jan 2012.

[37] Humberto González, Lluís Martínez-León, Fernando Soldevila, Ma. Araiza-Esquivel, Jesús Lancis, and Enrique Tajahuerce. High sampling rate single-pixel digital holography system employing a dmd and phase-encoded patterns. *Opt. Express*, 26(16):20342–20350, Aug 2018.

[38] M. Gross and M. Atlan. Digital holography with ultimate sensitivity. *Optics letters*, 32(8):909–911, 2007.

[39] N. Verrier, D. Alexandre, G. Tessier, and M. Gross. Holographic microscopy reconstruction in both object and image half-spaces with an undistorted three-dimensional grid. *Applied optics*, 54(15):4672–4677, 2015.

[40] F. Joud, F. Laloë, M. Atlan, J. Hare, and M. Gross. Imaging a vibrating object by sideband digital holography. *Opt. Express*, 17(4):2774–2779, Feb 2009.